What is a Quantum Shock Wave?

S. A. Simmons,[1] F. A. Bayocboc, Jr.,[1] J. C. Pillay,[1] D. Colas,[1,2] I. P. McCulloch,[1] and K. V. Kheruntsyan[1]
[1]School of Mathematics and Physics, University of Queensland, Brisbane, Queensland 4072, Australia
[2]ARC Centre of Excellence in Future Low-Energy Electronics Technologies, University of Queensland, Brisbane, Queensland 4072, Australia

(Received 24 June 2020; accepted 20 August 2020; published 26 October 2020)

Shock waves are examples of the far-from-equilibrium behavior of matter; they are ubiquitous in nature, yet the underlying microscopic mechanisms behind their formation are not well understood. Here, we study the dynamics of dispersive quantum shock waves in a one-dimensional Bose gas, and show that the oscillatory train forming from a local density bump expanding into a uniform background is a result of quantum mechanical self-interference. The amplitude of oscillations, i.e., the interference contrast, decreases with the increase of both the temperature of the gas and the interaction strength due to the reduced phase coherence length. Furthermore, we show that vacuum and thermal fluctuations can significantly wash out the interference contrast, seen in the mean-field approaches, due to shot-to-shot fluctuations in the position of interference fringes around the mean.

DOI: 10.1103/PhysRevLett.125.180401

Introduction.—The study of dispersive shock waves in superfluids, such as dilute gas Bose-Einstein condensates (BECs), has been attracting a growing attention in recent years (see, e.g., Refs. [1–10]). This is partly due to the fact that shock waves represent examples of far-from-equilibrium phenomena, for which a fundamental understanding of the laws of emergence from the underlying many-body interactions is generally lacking. Ultracold atomic gases offer a promising platform for addressing this open question due to the high level of experimental control over the system parameters and the dynamics. Other physical systems in which dispersive shock waves form, and which may benefit from such an understanding, include rarefield plasma [11,12], intense electron beams [13], liquid helium [14], and exciton polaritons [15].

Dispersive (or nondissipative) shock waves in fluid dynamics are identified by density ripples or oscillatory wave trains whose front propagates faster than the local speed of sound in the medium; a typical scenario for their formation is the expansion of a local density bump into a nonzero background. Dissipative shock waves, on the other hand, are characterised by a smooth but steep (nearly discontinuous) change in the density [1,16,17]. In either case, the effects of dispersion or dissipation prevent the unphysical hydrodynamic gradient catastrophe by means of energy transfer from large to small lengthscales, or through the release of the excess energy via damping.

While dissipative shock waves involve irreversible processes that can be well described within classical hydrodynamics, dispersive shock waves in BECs require quantum or superfluid hydrodynamics for their description. The latter can be derived from the mean-field description of weakly interacting BECs via the Gross-Pitaevskii equation (GPE) [18,19]. The effect of dispersion is represented here by the so-called quantum pressure term, hence the use of an alternative term for dispersive shock waves—quantum shock waves [2]. We point out, however, that essentially the same phenomenon can be observed in classical nonlinear optics [20,21], wherein the electromagnetic dispersive shock waves are generated in a medium with a Kerr-like nonlinearity and are described by the nonlinear Schrödinger equation (NLSE). The presence of nonlinear interaction [22], in both the GPE and NLSE, has been exploited in, and is required for, the interpretation of dispersive shock waves as a train of gray solitons [6,23]. However, as we show below, qualitatively similar density modulations can form in a noninteracting case which does not support solitons. These incongruencies imply that the understanding of dispersive shock waves requires reassessment, including clarification of the role of actual quantum and thermal fluctuations which require beyond-mean-field descriptions.

In this Letter, we study dispersive shock waves in a one-dimensional (1D) Bose gas, described by the Lieb-Liniger model [24], and show that the microscopic mechanism behind the formation of the oscillatory wave train is quantum mechanical interference: the wave packet that makes up a local density bump self-interferes with its own background upon expanding into it. This is in contrast to a Gaussian wave packet expanding into free space, which maintains its shape. Our results span the entire range of interaction strengths, from the noninteracting (ideal) Bose gas regime, through the weakly interacting or Gross-Pitaevskii regime, to the regime of infinitely strong interactions corresponding to the Tonks-Girardeau (TG) gas of hard-core bosons [25,26]. In all regimes, the interference

contrast decreases with the reduction of the local phase coherence length. Moreover, in the weakly interacting regime, where the interference contrast is typically high, we show that thermal and quantum fluctuations can dramatically reduce the contrast due to shot-to-shot fluctuations in the position of interference fringes.

Ideal Bose gas.—We begin our analysis with the simplest case of an ideal Bose gas. For analytical insight, we consider the initial wave function $\Psi(x,0)=\psi_{\rm bg}(1+\beta e^{-x^2/2\sigma^2})$, prepared prior to time $t=0$ as the ground state of a suitably chosen dimple potential, which subsequently evolves in a uniform potential of length L with periodic boundary conditions. The Gaussian bump has a width σ and amplitude β above a (real) constant background $\psi_{\rm bg}$ which fixes the normalization of the wave function to unity in the single-particle case, or to the total number of particles N in the system [27]. The dimensionless density $\bar{\rho}_{\rm bg}=\rho_{\rm bg}L=|\psi_{\rm bg}|^2L=N_{\rm bg}$ gives the number of particles in the background, with $N=N_{\rm bg}\{1+(\sqrt{\pi}\beta\sigma/L)[\beta{\rm erf}(L/2\sigma)+2\sqrt{2}{\rm erf}(L/2\sqrt{2}\sigma)]\}$. The wave function $\Psi(x,0)$ evolves according to the time-dependent Schrödinger equation, whose solution can be written as

$$\Psi(x,t)=\psi_{\rm bg}\left(1+\frac{\beta\sigma}{\sqrt{\sigma^2+i\hbar t/m}}e^{-x^2/2(\sigma^2+i\hbar t/m)}\right). \quad (1)$$

The corresponding density profile $\rho(x,t)=|\Psi(x,t)|^2$ is shown in Fig. 1(a) at different dimensionless times $\tau=t/t_0$ (and before significant reflections off the boundary), where $t_0=mL^2/\hbar$ is the timescale, and m is the mass of the particles. As we see, $\rho(x,t)$ displays all the known hallmarks of dispersive shock waves from the GPE (see below). In particular, the shock wave oscillations are chirped, with high-frequency and small-amplitude components located at the shock front. The wave function (1) can be rewritten as $\Psi(x,t)=\psi_{\rm bg}[1+B(x,t)e^{i\varphi(x,t)}]$, so that the density $\rho(x,t)=|\Psi(x,t)|^2$ acquires a textbook form of quantum mechanical interference, $\rho(x,t)=\psi_{\rm bg}^2[1+B(x,t)^2+2B(x,t)\cos\varphi(x,t)]$, with the amplitude $B(x,t)\equiv\{(\beta\sigma)/([\sigma^4+\hbar^2t^2/m^2]^{1/4})\}e^{-x^2\sigma^2/2[\sigma^4+\hbar^2t^2/m^2]}$ and phase $\varphi(x,t)\equiv\{(\hbar tx^2)/(2m[\sigma^4+\hbar^2t^2/m^2])\}-\frac{1}{2}{\rm atan}(\hbar^2t^2/m^2\sigma^4)$. This means that the period of oscillations in the bulk of the shock train is $\sim 2\sigma$ (with σ being the only relevant length scale in the problem), whereas the amplitude scales as $\propto\beta\sigma/\sqrt{t}$.

Weakly interacting Bose gas in the GPE regime.—We now move to consider repulsive pairwise delta-function interactions of strength g, and find ourselves in the realm of the Lieb-Liniger model [24,31,32]. For a uniform system, the relevant dimensionless interaction parameter is $\gamma=mg/\hbar^2\rho$, where ρ is the 1D density. For a nonuniform gas with a local density bump, one can introduce a local interaction parameter $\gamma(x)=mg/\hbar^2\rho(x)$ and use, e.g., the background value $\gamma_{\rm bg}=mg/\hbar^2\rho_{\rm bg}$ as the global interaction parameter to characterise the initial state (in addition to specifying the height and width of the bump). The weakly interacting regime of the Lieb-Liniger gas corresponds to $\gamma_{\rm bg}\ll 1$ [hence $\gamma(x)\ll 1$ at any other x within the bump], and the zero-temperature ($T=0$) dynamics of the system can be approximated by the GPE for the complex mean-field amplitude $\Psi(x,t)$:

$$i\hbar\partial_t\Psi(x,t)=\left(-\frac{\hbar^2}{2m}\partial_{xx}+g|\Psi(x,t)|^2\right)\Psi(x,t). \quad (2)$$

Dispersive shock waves forming under the GPE are shown in Figs. 1(b) and 1(c), and are qualitatively similar to those in the ideal Bose gas. The interfering nature of the density ripples in this regime, where we no longer have an explicit analytic solution, can be revealed [32] via a wavelet transform known from signal processing theory [33–36]. The only difference that arises here is that the interaction term in the GPE sets up a new lengthscale in the problem—the healing length $l_h=\hbar/\sqrt{mg\rho_{\rm bg}}$ of the background. The healing length decreases with increasing interactions, and

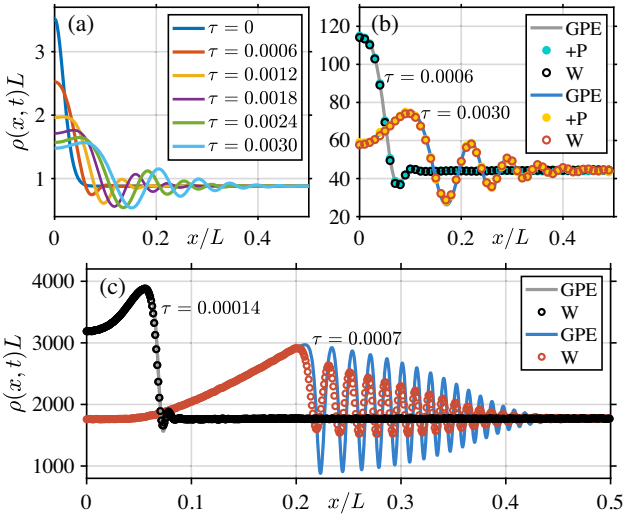

FIG. 1. Dispersive shock waves in an ideal and weakly interacting 1D Bose gas at $T=0$. In (a), we show the single-particle probability densities $\rho(x,t)=|\Psi(x,t)|^2$ for the ideal gas at different dimensionless times τ, for $\beta=1$ and $\sigma/L=0.02$. Due to the reflectional symmetry about the origin, we only show the densities for $x>0$. In (b) and (c), we show the density profiles in the weakly interacting regime at two instances of time, with the GPE simulations represented by solid (grey and blue) lines. We also show the results of stochastic phase-space simulations [28] using the truncated Wigner (W) and positive-P ($+P$) approaches, which incorporate the effects of vacuum fluctuations (see text). The shape of $\rho(x,0)$ (not shown) in (b) and (c) is the same as in (a), except that it is now normalized to N: (b) $N=50$, $\gamma_{\rm bg}=0.1$; (c) $N=2000$, $\gamma_{\rm bg}=0.01$ [30]. The dimensionless healing length $l_h/L=1/\sqrt{\gamma_{\rm bg}N_{\rm bg}}$ is $l_h/L\simeq 0.072$ in (b), and $l_h/L\simeq 0.0057$ in (c), which can be compared to $\sigma/L=0.02$.

as soon as it becomes the shortest lengthscale in the problem (hence determining the effective UV momentum cutoff) it overtakes the role of σ in determining the characteristic period of interference oscillations. An example of this scenario is shown in Fig. 1(c): here, the initial density profile is in the Thomas-Fermi regime (where the mean-field interaction energy per particle is much larger than the kinetic energy) with $l_h < \sigma$, and the characteristic period of oscillations is $\sim 2l_h$. The trailing interference fringe of the shock wave train propagates approximately at the speed of sound $c_s = \sqrt{g\rho_{\rm bg}/m}$ at the background density $\rho_{\rm bg}$, obtained from the Bogolibov spectrum of elementary excitations [24].

The GPE can be equivalently formulated in terms of superfluid hydrodynamics via Madelung's transformation to the density and phase variables, $\Psi(x,t) = \sqrt{\rho(x,t)}e^{i\phi(x,t)}$, and the velocity field $v(x,t) = (\hbar/m)\partial_x\phi(x,t)$, which yields

$$\partial_t \rho = -\partial_x(\rho v), \tag{3}$$

$$\partial_t v = -\partial_x\left(\frac{1}{2}v^2 + \frac{g\rho}{m} - \frac{\hbar^2}{2m^2}\frac{1}{\sqrt{\rho}}\partial_{xx}\sqrt{\rho}\right). \tag{4}$$

The last (dispersive) term in Eq. (4) is referred to as the quantum pressure term; it is this term that governs the formation of the oscillatory wave train in the hydrodynamic approach.

The same quantum pressure term arises in the hydrodynamiclike formulation of the single-particle Schrödinger equation after applying Madelung's transformation to the quantum mechanical wave function. This means that in the ideal Bose gas case, with $g = 0$ in the above hydrodynamic equations, it is again the quantum pressure term that is responsible for producing dispersive shock wave oscillations in Fig. 1(a). We note then, that the interaction g is not necessary for the formation of the oscillatory shock wave train, and as such these oscillations cannot generally be interpreted as a train of gray solitons [6,23] that do require the interactions to balance the wave dispersion.

Strongly interacting and Tonks-Girardeau regimes.— We now extend our analysis to increasingly stronger interaction strengths, from $\gamma_{\rm bg} \sim 1$ to the TG limit of $\gamma_{\rm bg} \to \infty$ [24–26]. The shock wave dynamics in this regime are shown in Fig. 2 and are simulated using infinite matrix product states (iMPS) [32], starting from the ground state of a dimple potential $V(x)$. The key observation here is that the amplitude of shock wave oscillations (i.e., the interference contrast) goes down with increasing $\gamma_{\rm bg}$ due to the reduction of the local phase coherence length of the gas. The phase coherence length of a 1D Bose gas crosses over from essentially the size of the system in the GPE regime down to the mean interparticle separation $1/\rho_{\rm bg}$ in the limit of $\gamma_{\rm bg} \gg 1$ [72]. Furthermore, for $\gamma_{\rm bg} \gg 1$, the initial ground state density profile exhibits small-amplitude Friedel oscillations [73], with a characteristic period equal to the mean interparticle separation $1/\rho_{\rm bg}$. This means that discerning between the deformations of these preexisting oscillations and shock wave interference fringes, which form dynamically, becomes ambitious especially when the width σ is on the same order of magnitude as $1/\rho_{\rm bg}$.

These observations become more evident in the TG limit of $\gamma_{\rm bg} \to \infty$, where the mean interparticle separation in the background becomes the shortest length scale in the problem, related to the Fermi wavelength $\lambda_F = 2\pi/k_F$ (with $k_F = \pi\rho_{\rm bg}$ being the Fermi wave vector at the background density) via $1/\rho_{\rm bg} = \lambda_F/2$. Examples of evolving density profiles in the TG limit, obtained using exact diagonalization of a free fermion Hamiltonian and iMPS simulations [32], are shown in Figs. 2(d) and 2(e) for a relatively wide and a very narrow density bump. As we see in Fig. 2(d), dispersive shock wave oscillations in the TG gas do not form [74] when the width of the bump σ is larger

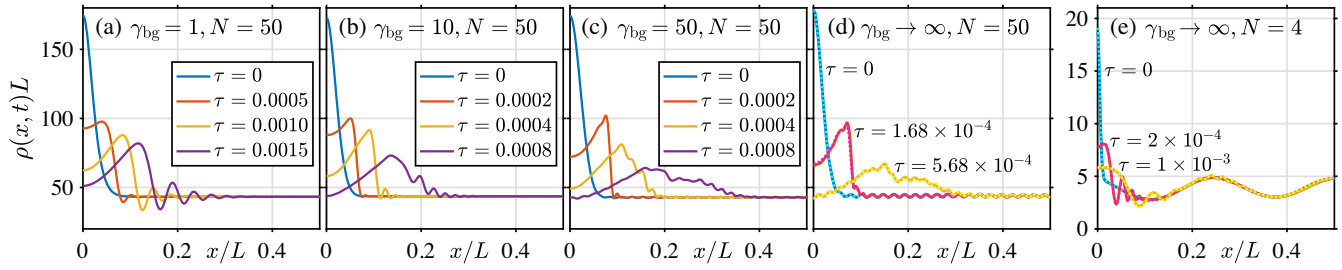

FIG. 2. Shock waves in a 1D Bose gas at $T = 0$ for intermediate and strong interactions. In all panels, the iMPS simulation results are shown as full lines; in (d) and (e), the iMPS results are compared with exact diagonalization results (dotted lines), and show excellent agreement. In (a)–(c), the trapping potential is chosen as $\bar{V}(\xi) = -\bar{V}_{\rm bg}[1 + \beta\exp(-\xi^2/2\bar{\sigma}^2)]^2$, with $\bar{\sigma} = 0.02$ in all cases, and: (a) $\beta = 0.98$, $\bar{V}_{\rm bg} = 1849$ (resulting in $N_{\rm bg} \simeq 43.2$); (b) $\beta = 0.7$, $\bar{V}_{\rm bg} = 18705$ ($N_{\rm bg} \simeq 43.6$); (c) $\beta = 0.38$, $\bar{V}_{\rm bg} = 92450$ ($N_{\rm bg} \simeq 43$). Here, $\bar{V}(\xi) \equiv V(x)/E_0$, with $E_0 = \hbar^2/mL^2$ being the energy scale. In (d), the trapping potential is chosen according to Eq. (S33) of [32], with $N_{\rm bg} = 44.03$, $\beta = 1$, and $\bar{\sigma} = 0.02$; in the Thomas-Fermi approximation, this would produce exactly the same initial density profile as in Fig. 1(a), which, however, would not display the Friedel oscillations seen here. In (e), the trapping potential has the same shape as the one used for producing the ideal Bose gas initial density profile of Fig. 1(a), except normalized to $N = 4$.

than the phase coherence length $1/\rho_{\rm bg}$. The small density ripples seen in this case are simply evolving deformations of the initial Friedel oscillations [75]. When, however, $\sigma < 1/\rho_{\rm bg}$, as in Fig. 2(e), we do observe small-scale dispersive shock waves, confined initially within a single Friedel-oscillation period of $1/\rho_{\rm bg} = \lambda_F/2$. The characteristic period of interference fringes in this case is determined by σ as it is now the shortest length scale in the problem.

The effects of thermal and vacuum fluctuations.—In order to understand the effect of thermal fluctuations on dispersive shock waves, we consider the finite temperature quasicondensate regime of the 1D Bose gas [37,44,69,76–78]. This regime still corresponds to weak interactions, $\gamma_{\rm bg} \ll 1$, but we focus on temperatures of the initial thermal state lying within $\gamma_{\rm bg} \lesssim \bar{T} \lesssim \sqrt{\gamma_{\rm bg}}$ [69,77], where $\bar{T} = T/T_d$ is the dimensionless temperature, $T_d = \hbar^2\rho_{\rm bg}^2/2mk_B$ is the temperature of quantum degeneracy of the gas at density $\rho_{\rm bg}$, and k_B is the Boltzmann constant [79]. In this range of temperatures, which are most readily accessible in ultracold atom experiments [78,80,81], the density-density correlations of the gas are dominated by thermal rather than vacuum fluctuations [69,77]. Accordingly, the shock wave dynamics can be simulated using c-field techniques 47–45]], which involve preparation of the initial thermal equilibrium state using the stochastic projected Gross-Pitaevskii equation (SPGPE) and subsequent real-time evolution according to the GPE.

Examples of SPGPE simulations are shown in Fig. 3 for the same parameters as in Fig. 1(c), but for two nonzero temperatures. As expected, the interference contrast is significantly reduced (compared to GPE results) due to thermal fluctuations and the resulting loss of phase coherence. Indeed, in the quasicondensate regime with density $\rho_{\rm bg}$, the thermal phase coherence length is given by $l_T = \hbar^2\rho_{\rm bg}/mk_BT$. From this estimate one can expect that the self-interfering shock wave train would lose its contrast when l_T becomes on the order of or smaller than the width of the bump σ, with oscillations eventually disappearing at sufficiently high temperatures. This is indeed what we see in Fig. 3. However, the interference contrast in the example of Fig. 3(a) is essentially lost at temperatures for which l_T is still larger than σ; this can be explained by the shot-to-shot fluctuations in the position of interference fringes due to the same thermal fluctuations. Indeed, as can be seen from samples of individual stochastic SPGPE trajectories (shown as thin lines), even though these individual trajectories show high-contrast interference fringes (albeit with stochastic noise also present), the overall ensemble average over thousands of SPGPE realizations shows much lower interference contrast. This observation is consistent with the interpretation of the individual SPGPE trajectories representing individual experimental runs [47], whereas the mean density corresponds to the ensemble average over many runs.

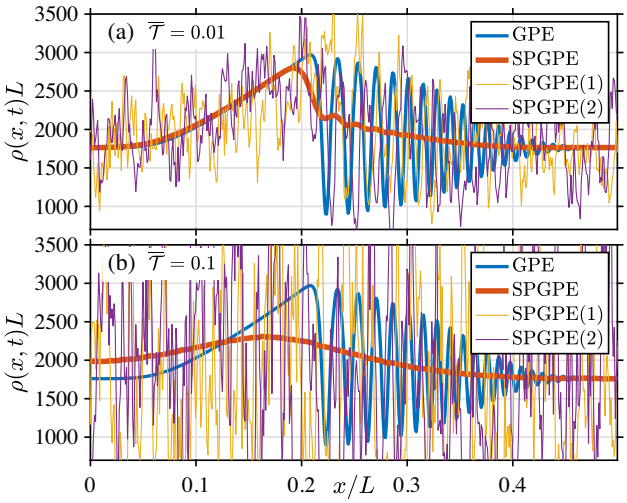

FIG. 3. Shock waves in a finite-temperature quasicondensate from SPGPE simulations (thick red lines). Shown are the final-time ($\tau = 0.0007$) density distributions for $x > 0$ and two different initial dimensionless temperatures: (a) $\bar{T} = 0.01$, and (b) $\bar{T} = 0.1$ [79]. Other parameters are as in Fig. 1 (c); the GPE results are shown here again as blue lines for comparison. The dimensionless thermal phase coherence length here can be expressed as $l_T/L = 2/(\bar{T}N_{\rm bg})$, giving: (a) $l_T/L \simeq 0.1$, (b) $l_T/L \simeq 0.01$. The SPGPE mean densities are the averages over 100 000 stochastic trajectories, whereas the thin lines show two sample trajectories.

Finally, we consider the effect of quantum fluctuations on the shock wave interference contrast in the weakly interacting regime at $T = 0$. These are treated using two stochastic phase-space methods, the truncated Wigner and positive-P approaches [48], and the iMPS method. The stochastic simulation results are shown in Figs. 1(b) and 1(c), and are directly comparable to those based on the mean-field GPE. For the parameters of Fig. 1(b) (very weak interactions), the truncated Wigner and positive-P results agree with each other (in addition to being in excellent agreement with iMPS results [32]) within the respective error bars, and are close to the GPE results. In this regime, the quantum fluctuations have a negligible effect on the mean density and the interference contrast. For the parameters of Fig. 1(c), on the other hand, the interactions are stronger (with the period of shock wave oscillations determined by l_h rather than σ) and the quantum fluctuations have a more profound effect: the interference contrast is visibly reduced compared to the GPE prediction [82]. This is similar to the effect of thermal fluctuations discussed above, and can be attributed to shot-to-shot fluctuations in the position of interference fringes around the mean.

Conclusions.—We have shown that the mechanism of formation of dispersive shock wave trains in a 1D Bose gas is quantum interference: the local perturbation self-interferes with its own background upon expanding into it. The interference contrast in this picture goes down with

the reduction of the phase coherence length of the gas, and the picture holds true for all interaction strengths. We have also shown that thermal and quantum fluctuations can reduce the interference contrast further due to shot-to-shot fluctuations in the position of interference fringes around the mean. In the TG limit of infinitely strong interactions, where the phase coherence length is the same as the mean interparticle separation, the shock wave oscillations are absent for a sufficiently wide density bump (wider than the mean interparticle separation). Apart from explaining the origin of density ripples in dispersive quantum shock waves, our results may serve as a test bed for new theoretical and computational techniques for many-body dynamics, such as the generalized hydrodynamics [83–86], and may shed new light on the understanding of dispersive shock waves in a variety of other contexts, such as in electronic systems described by the Calogero-Sutherland model and Korteweg–de Vries equations [1,8,87], or superfluids with higher-order dispersion [88].

K. V. K. acknowledges stimulating discussions with A. G. Abanov, V. V. Cheianov, J. F. Corney, M. J. Davis, and D. M. Gangardt. This work was supported through Australian Research Council (ARC) Discovery Project Grants No. DP170101423 and No. DP190101515, and by the ARC Centre of Excellence in Future Low-Energy Electronics Technologies (Project No. CE170100039).

[1] G. El and M. Hoefer, Physica (Amsterdam) **333D**, 11 (2016).
[2] Z. Dutton, M. Budde, C. Slowe, and L. V. Hau, Science **293**, 663 (2001).
[3] B. Damski, Phys. Rev. A **69**, 043610 (2004).
[4] T. P. Simula, P. Engels, I. Coddington, V. Schweikhard, E. A. Cornell, and R. J. Ballagh, Phys. Rev. Lett. **94**, 080404 (2005).
[5] M. A. Hoefer, M. J. Ablowitz, I. Coddington, E. A. Cornell, P. Engels, and V. Schweikhard, Phys. Rev. A **74**, 023623 (2006).
[6] J. J. Chang, P. Engels, and M. A. Hoefer, Phys. Rev. Lett. **101**, 170404 (2008).
[7] R. Meppelink, S. B. Koller, J. M. Vogels, P. van der Straten, E. D. van Ooijen, N. R. Heckenberg, H. Rubinsztein-Dunlop, S. A. Haine, and M. J. Davis, Phys. Rev. A **80**, 043606 (2009).
[8] M. Kulkarni and A. G. Abanov, Phys. Rev. A **86**, 033614 (2012).
[9] A. Bulgac, Y.-L. Luo, and K. J. Roche, Phys. Rev. Lett. **108**, 150401 (2012).
[10] S. Peotta and M. DiVentra, Phys. Rev. A **89**, 013621 (2014).
[11] R. J. Taylor, D. R. Baker, and H. Ikezi, Phys. Rev. Lett. **24**, 206 (1970).
[12] M. Q. Tran, K. Appert, C. Hollenstein, R. W. Means, and J. Vaclavik, Plasma Phys. **19**, 381 (1977).
[13] Y. C. Mo, R. A. Kishek, D. Feldman, I. Haber, B. Beaudoin, P. G. O'Shea, and J. C. T. Thangaraj, Phys. Rev. Lett. **110**, 084802 (2013).
[14] E. Rolley, C. Guthmann, and M. Pettersen, Physica (Amsterdam) **394B**, 46 (2007).
[15] L. Dominici, M. Petrov, M. Matuszewski, D. Ballarini, M. De Giorgi, D. Colas, E. Cancellieri, B. S. Fernández, A. Bramati, G. Gigli *et al.*, Nat. Commun. **6**, 8993 (2015).
[16] N. K. Lowman and M. A. Hoefer, Phys. Rev. A **88**, 013605 (2013).
[17] M. E. Mossman, M. A. Hoefer, K. Julien, P. G. Kevrekidis, and P. Engels, Nat. Commun. **9**, 4665 (2018).
[18] F. Dalfovo, S. Giorgini, L. P. Pitaevskii, and S. Stringari, Rev. Mod. Phys. **71**, 463 (1999).
[19] C. Pethick and H. Smith, *Bose-Einstein Condensation in Dilute Gases* (Cambridge University Press, Cambridge, England, 2001).
[20] J. E. Rothenberg and D. Grischkowsky, Phys. Rev. Lett. **62**, 531 (1989).
[21] W. Wan, S. Jia, and J. W. Fleischer, Nat. Phys. **3**, 46 (2007).
[22] The term "nonlinear interaction" in the NLSE or GPE refer, respectively, to the Kerr (or $\chi^{(3)}$) interaction induced by the nonlinear optical material, or to the *s*-wave scattering interaction (g) of the atomic BEC. This should not be confused with the nonlinear terms (with respect to the density and velocity fields) that arise in the partial differential equations in the equivalent hydrodynamic formulation of the problem; such nonlinear terms in the hydrodynamic equations are present even in the absence of any Kerr or *s*-wave interactions.
[23] M. Hoefer, P. Engels, and J. Chang, Physica (Amsterdam) **238D**, 1311 (2009).
[24] E. H. Lieb and W. Liniger, Phys. Rev. **130**, 1605 (1963); E. H. Lieb, Phys. Rev. **130**, 1616 (1963).
[25] M. Girardeau, J. Math. Phys. (N.Y.) **1**, 516 (1960).
[26] M. D. Girardeau, Phys. Rev. **139**, B500 (1965).
[27] We note that the precise details of the shape of the initial density profile with a local bump do not affect our main results and conclusions.
[28] In all stochastic simulations, performed using the XMDS software package of Ref. [29], the averages are over 100 000 stochastic trajectories and the standard error on the mean density is smaller than the radius of the circles.
[29] G. R. Dennis, J. J. Hope, and M. T. Johnsson, Comput. Phys. Commun. **184**, 201 (2013).
[30] For the parameters of Fig. 1(b), $N_{\rm bg} = 44.03$, and the dimensionless nonlinearity $\bar{g} = gmL/\hbar^2 = \gamma_{\rm bg} N_{\rm bg}$ in the GPE is $\bar{g} = 4.403$; similarly, for the parameters of Fig. 1(c), $N_{\rm bg} = 1761$ and $\bar{g} = 17.61$.
[31] M. Olshanii, Phys. Rev. Lett. **81**, 938 (1998).
[32] See the Supplemental Material at http://link.aps.org/supplemental/10.1103/PhysRevLett.125.180401 for the details of the Lieb-Liniger model [24,31], the wavelet transform [33–36], and the various theoretical and computational approaches used in our study: the mean-field GPE, modified GPE, and the associated hydrodynamic approaches [37–43]; *c*-field methods based on the SPGPE [37,44–47]; truncated Wigner and positive-*P* methods [47–54]; iMPS [55–68]; and exact diagonalization in the TG regime [25,69–71].
[33] C. H. Baker, D. A. Jordan, and P. M. Norris, Phys. Rev. B **86**, 104306 (2012).
[34] B. P. Abbott *et al.* (LIGO Scientific and Virgo Collaborations), Phys. Rev. Lett. **116**, 061102 (2016).

[35] D. Colas and F. P. Laussy, Phys. Rev. Lett. **116**, 026401 (2016).
[36] D. Colas, F. P. Laussy, and M. J. Davis, Phys. Rev. Lett. **121**, 055302 (2018).
[37] I. Bouchoule, S. S. Szigeti, M. J. Davis, and K. V. Kheruntsyan, Phys. Rev. A **94**, 051602(R) (2016).
[38] M. D. Girardeau and E. M. Wright, Phys. Rev. Lett. **84**, 5239 (2000).
[39] Y. Y. Atas, D. M. Gangardt, I. Bouchoule, and K. V. Kheruntsyan, Phys. Rev. A **95**, 043622 (2017).
[40] Y. Y. Atas, I. Bouchoule, D. M. Gangardt, and K. V. Kheruntsyan, Phys. Rev. A **96**, 041605(R) (2017).
[41] B. Damski, Phys. Rev. A **73**, 043601 (2006).
[42] E. B. Kolomeisky, T. J. Newman, J. P. Straley, and X. Qi, Phys. Rev. Lett. **85**, 1146 (2000).
[43] S. Choi, V. Dunjko, Z. D. Zhang, and M. Olshanii, Phys. Rev. Lett. **115**, 115302 (2015).
[44] I. Bouchoule, M. Arzamasovs, K. V. Kheruntsyan, and D. M. Gangardt, Phys. Rev. A **86**, 033626 (2012).
[45] Y. Castin, R. Dum, E. Mandonnet, A. Minguzzi, and I. Carusotto, J. Mod. Opt. **47**, 2671 (2000).
[46] M. J. Davis, S. A. Morgan, and K. Burnett, Phys. Rev. Lett. **87**, 160402 (2001).
[47] P. B. Blakie, A. S. Bradley, M. J. Davis, R. J. Ballagh, and C. W. Gardiner, Adv. Phys. **57**, 363 (2008).
[48] M. J. Steel, M. K. Olsen, L. I. Plimak, P. D. Drummond, S. M. Tan, M. J. Collett, D. F. Walls, and R. Graham, Phys. Rev. A **58**, 4824 (1998).
[49] A. D. Martin and J. Ruostekoski, New J. Phys. **12**, 055018 (2010).
[50] P. D. Drummond and C. W. Gardiner, J. Phys. A **13**, 2353 (1980).
[51] A. Gilchrist, C. W. Gardiner, and P. D. Drummond, Phys. Rev. A **55**, 3014 (1997).
[52] C. M. Savage, P. E. Schwenn, and K. V. Kheruntsyan, Phys. Rev. A **74**, 033620 (2006).
[53] P. Deuar and P. D. Drummond, Phys. Rev. Lett. **98**, 120402 (2007).
[54] A. Perrin, C. M. Savage, D. Boiron, V. Krachmalnicoff, C. I. Westbrook, and K. V. Kheruntsyan, New J. Phys. **10**, 045021 (2008).
[55] S. R. White, Phys. Rev. Lett. **69**, 2863 (1992).
[56] I. P. McCulloch, J. Stat. Mech. (2007) P10014.
[57] U. Schollwck, Ann. Phys. (Amsterdam) **326**, 96 (2011).
[58] M. A. Cazalilla, Phys. Rev. A **67**, 053606 (2003).
[59] B. Schmidt, L. I. Plimak, and M. Fleischhauer, Phys. Rev. A **71**, 041601(R) (2005).
[60] B. Schmidt and M. Fleischhauer, Phys. Rev. A **75**, 021601 (R) (2007).
[61] D. Muth, B. Schmidt, and M. Fleischhauer, New J. Phys. **12**, 083065 (2010).
[62] D. Muth, M. Fleischhauer, and B. Schmidt, Phys. Rev. A **82**, 013602 (2010).
[63] I. P. McCulloch, arXiv:0804.2509.
[64] H. N. Phien, G. Vidal, and I. P. McCulloch, Phys. Rev. B **86**, 245107 (2012).
[65] G. Vidal, Phys. Rev. Lett. **98**, 070201 (2007).
[66] A. J. Daley, C. Kollath, U. Schollwöck, and G. Vidal, J. Stat. Mech. (2004) P04005.
[67] S. R. White and A. E. Feiguin, Phys. Rev. Lett. **93**, 076401 (2004).
[68] T. Barthel and Y. Zhang, Ann. Phys. (Amsterdam) **418**, 168165 (2020).
[69] K. V. Kheruntsyan, D. M. Gangardt, P. D. Drummond, and G. V. Shlyapnikov, Phys. Rev. A **71**, 053615 (2005).
[70] V. Yukalov and M. Girardeau, Laser Phys. Lett. **2**, 375 (2005).
[71] D. J. Griffiths, *Introduction to Quantum Mechanics* (Prentice Hall International, Englewood Cliffs, NJ, 1994).
[72] M. A. Cazalilla, J. Phys. B **37**, S1 (2004).
[73] J. Friedel, Nuovo Cimento (1955–1965) **7**, 287 (1958).
[74] Absence of dispersive shock wave oscillations in the Tonks limit has been conjectured in Ref. [8]. The trailing edge of the shock wave envelope in this limit propagates approximately at the respective speed of sound at the background density, $v_s = \pi\hbar\rho_{\rm bg}/m$ [24].
[75] This is in stark contrast to the predictions of a hydrodynamiclike description of the TG gas [41], equivalent to a modified GPE with a quartic, rather than quadratic, nonlinear term [38,42,43], in which the interference contrast appears similarly high (see [32]) to that in the weakly interacting GPE regime.
[76] D. S. Petrov, G. V. Shlyapnikov, and J. T. M. Walraven, Phys. Rev. Lett. **85**, 3745 (2000).
[77] K. V. Kheruntsyan, D. M. Gangardt, P. D. Drummond, and G. V. Shlyapnikov, Phys. Rev. Lett. **91**, 040403 (2003).
[78] T. Jacqmin, J. Armijo, T. Berrada, K. V. Kheruntsyan, and I. Bouchoule, Phys. Rev. Lett. **106**, 230405 (2011).
[79] The dimensionless temperature parameters $\bar{\mathcal{T}}$ and $\bar{T} = k_B T/E_0$ (with $E_0 = \hbar^2/mL^2$) are related by $\bar{\mathcal{T}} = 2\bar{T}/\bar{\rho}_{\rm bg}^2 = 2\bar{T}/N_{\rm bg}^2$.
[80] A. H. van Amerongen, J. J. P. van Es, P. Wicke, K. V. Kheruntsyan, and N. J. van Druten, Phys. Rev. Lett. **100**, 090402 (2008).
[81] I. Bouchoule, N. J. van Druten, and C. I. Westbrook, Atom chips and one-dimensional Bose gases, in *Atom Chips* (Wiley-VCH Verlag GmbH & Co. KGaA, New York, 2011), pp. 331–363.
[82] For the parameters of Fig. 1(b), the iMPS results are in excellent agreement with the truncated Wigner and positive-P results, and are omitted from the figure for clarity, whereas for the parameters of Fig. 1(c), the iMPS method is computationally intractable due to the large number of particles in the system. The positive-P approach for Fig. 1(c) is similarly computationally intractable due to large sampling errors.
[83] B. Doyon, J. Dubail, R. Konik, and T. Yoshimura, Phys. Rev. Lett. **119**, 195301 (2017).
[84] O. A. Castro-Alvaredo, B. Doyon, and T. Yoshimura, Phys. Rev. X **6**, 041065 (2016).
[85] B. Bertini, M. Collura, J. De Nardis, and M. Fagotti, Phys. Rev. Lett. **117**, 207201 (2016).
[86] R. Dubessy, J. Polo, H. Perrin, A. Minguzzi, and M. Olshanii, arXiv:2007.05252 [Phys. Rev. Lett. (to be published)].
[87] E. Bettelheim, A. G. Abanov, and P. Wiegmann, Phys. Rev. Lett. **97**, 246401 (2006).
[88] M. E. Mossman, E. S. Delikatny, M. M. Forbes, and P. Engels, arXiv:2004.00832.